ChemComm

COMMUNICATION

View Article Online
View Journal | View Issue

Cite this: *Chem. Commun.*, 2025, **61**, 13117

Received 13th May 2025,
Accepted 25th July 2025

DOI: 10.1039/d5cc02654g

rsc.li/chemcomm

Origin of the red-shifted absorption maximum in channelrhodopsin Chrimson†

Jonathan R. Church, ‡[a] Probal Nag, ‡[ab] Tal Dogon[a] and Igor Schapiro *[abc]

Chrimson is a naturally occurring channelrhodopsin with one of the most red-shifted absorption maxima (λ_{max} = 590 nm). This unique absorption makes it an ideal candidate for noninvasive optogenetic applications. The origin of the absorption maximum is thought to stem from a single deprotonated counterion near the Schiff base. However, it remains unclear which of the two potential counterions, E165 and D295, is protonated. In addition, a third titratable residue (E132) near the chromophore may also play a role in the spectral tuning mechanism. A single mutation from serine to alanine (S169A) further red-shifts the absorption maximum to 608 nm. Here we elucidate the mechanism behind the red-shifted absorption maximum using classical molecular dynamics simulations in tandem with hybrid QM/MM simulations. We found that protonation of both E165 and E132 leads to the correct experimental absorption trend for the wild type. This was further validated for the S169A mutant. The derived understanding of the spectral shift will guide the experimental design of red-shifted microbial rhodopsins.

Channelrhodopsins are light-activated ion channels, making them ideal candidates for biotechnological applications such as optogenetics or vision restoration.[1–3] These are part of the rhodopsin protein superfamily which gains its light sensitivity from a covalently bound retinal chromophore. The chromophore is linked to the opsin through a lysine residue (Fig. 1). Together, the lysine and retinal chromophore form a retinal protonated Schiff base (RPSB), which is positively charged. Hence, the absorption of the chromophore is influenced by the surrounding protein environment. The range of absorption maxima found in rhodopsins spans from 400 nm to 690 nm.[4–14] In particular, variants absorbing in the red portion of the visible spectrum are of high interest in biotechnology because of the deep tissue penetration within the biological transparency window from 650 nm to 950 nm.

A channelrhodopsin Chrimson, discovered in 2014 in the algae *Chlamydomonas noctigama*, showed a red-shifted absorption maximum (λ_{max} = 590 nm) compared to the other variants.[15] This is of particular interest, as its unique absorption has recently been used within a dual-color optogenetic tool to control neuronal activity[3,16,17] and aid in restoring vision and hearing.[1,18]

Oda *et al.* have solved the crystal structure of Chrimson at a resolution of 2.6 Å, allowing atomistic insight, making it the most red-shifted channelrhodopsin with an available structure.[19] Analysis of the crystal structure revealed that the binding pocket of Chrimson is similar to that of other channelrhodopsins. There are two counterions, E165 and D295 (counterions 1 and 2, respectively), located within 3.6 Å of the

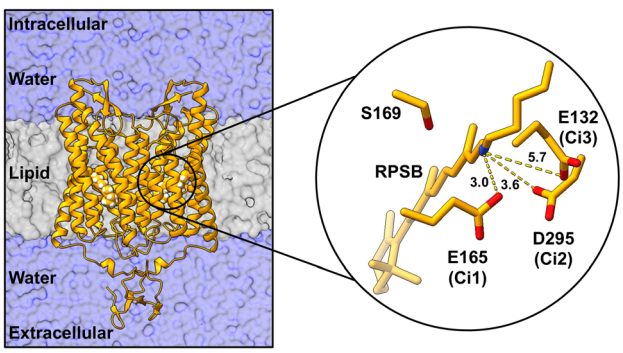

Fig. 1 Dimeric channelrhodopsin Chrimson embedded in a lipid bilayer in the simulation box. The inset shows a zoom of the binding pocket containing the retinal chromophore and lysine link (RPSB) of a Chrimson monomer, including several key residues mentioned in this study: S169 and E165 (Ci1), D295 (Ci2) and E132 (Ci3). The distance between the nitrogen atom of the Schiff base moiety and the oxygen atoms of charged residues is provided in Å.

[a] *Fritz Haber Center for Molecular Dynamics Research, Institute of Chemistry, The Hebrew University of Jerusalem, Jerusalem 9190401, Israel. E-mail: Igor.Schapiro@tu-dortmund.de*
[b] *Department of Physics, Technical University Dortmund, 44227 Dortmund, Germany*
[c] *Research Center Chemical Sciences and Sustainability, University Alliance Ruhr, 44801 Bochum, Germany*

† Electronic supplementary information (ESI) available: Computational methodology, Tables S1–S3, and Fig. S1–S5 as mentioned in the text. See DOI: https://doi.org/10.1039/d5cc02654g

‡ These authors contributed equally.

protonated Schiff base moiety (Fig. 1). Additionally, a third titratable glutamate, E132 (potential counterion 3), is also located within 5.7 Å to the Schiff base. These negatively charged residues can greatly influence the absorption properties of Chrimson. A further red shift of the maximum absorption by 18 nm to λ_{max} = 608 nm was obtained by a single point mutation from serine to alanine at position 169 (S169A variant).

Spectral tuning of rhodopsins has often been explained by using the point charge model of Honig *et al.*[20–22] This mechanism is based on the intramolecular charge redistribution in the chromophore upon excitation. The positive charge of the chromophore, initially localized near the protonated Schiff base moiety in the ground state, translocates towards the β-ionone ring upon excitation. This charge redistribution allows residues on either side of the chromophore to impact the spectral tuning of the protein (Fig. 2). For example, a negative charge near the Schiff base will have a larger stabilizing effect on the ground state than the excited state, leading to a blue-shifted absorption maximum.

Based on this mechanism, it was hypothesized that the red-shifted absorption maximum in Chrimson originated from a reduced negative charge next to the Schiff base. This means a single unprotonated counterion, in contrast to other channelrhodopsins that have two unprotonated counterions. However, it remains unclear which of the two counterions, E165 or D295, is protonated despite the high-resolution crystal structure. Recent studies suggest that protonation of the E165 residue plays a key role in the unique absorption maximum of this protein.[23,24] Furthermore, the protonation state of E132 and the role of this residue are not known. Hence, it is imperative to identify the protonation state of the titratable residues to test the proposed spectral tuning mechanism.

The protonation states of such residues have been investigated computationally in microbial rhodopsins.[25–31] In the automatic rhodopsin modelling (ARM) protocol by Olivucci and coworkers, the protonation state of the major and secondary counterions was shown to be the key to improving the description of outliers.[32] Pieri *et al.* have performed constant pH simulations to identify the residues responsible for the spectral shifts depending on the pH titration.[33]

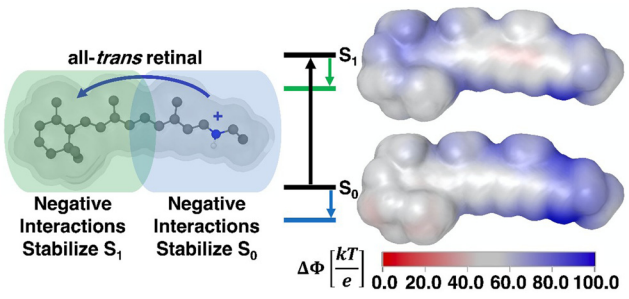

Fig. 2 Point charge model for retinal protonated Schiff base. The electrostatic potential ($\Delta\Phi$) is shown according to the map in kT e^{-1} units. The schematic shows that the positive charge of retinal in the ground state (S_0) is localized near the Schiff base. Upon excitation to S_1, there is a redistribution of the positive charge towards the β-ionone ring.

Table 1 Four protonation models examined for wild-type Chrimson and the S169A mutant. The name of the model denotes which counterions are protonated

Residue	P1	P2	P1&3	P2&3
E165 (Ci1)	✓	—	✓	—
D295 (Ci2)	—	✓	—	✓
E132 (Ci3)	—	—	✓	✓

In this work, we use multiscale simulations to probe the protonation state of E165 (Ci1), D295 (Ci2), and E132 (Ci3). Four protonation models were studied (Table 1). Two models have either Ci1 or Ci2 protonated, while Ci3 remains deprotonated. In addition, two models were added where Ci3 was also protonated. For each model, we first performed classical molecular dynamics (MD) simulations of Chrimson embedded in the membrane, followed by hybrid quantum mechanics/molecular mechanics (QM/MM) calculations.[34,35] The S169A mutant of Chrimson was also examined under the four protonation patterns. This helped validate the computational model and understand the origin of the red shift.

The root-mean-squared deviation (RMSD) for the three residues in the wild-type and the S169A mutant was analyzed for each trajectory (Fig. S1 and S3 (ESI†), respectively) relative to the experimental crystal structure. Similarly, the RMSD for the protein, the chromophore binding pocket, and the retinal chromophore were also examined to evaluate the overall stability of the protein (Fig. S2 and S4, ESI†).

The RMSD analysis of each model shows that changing the protonation of the three titratable residues can lead to large structural changes both locally in terms of the binding pocket and for the protein as a whole (Fig. S2, ESI†). Protonation of E132 produced smaller RMSD fluctuations regardless of whether E165 or D295 was protonated (P1&3 and P2&3). The

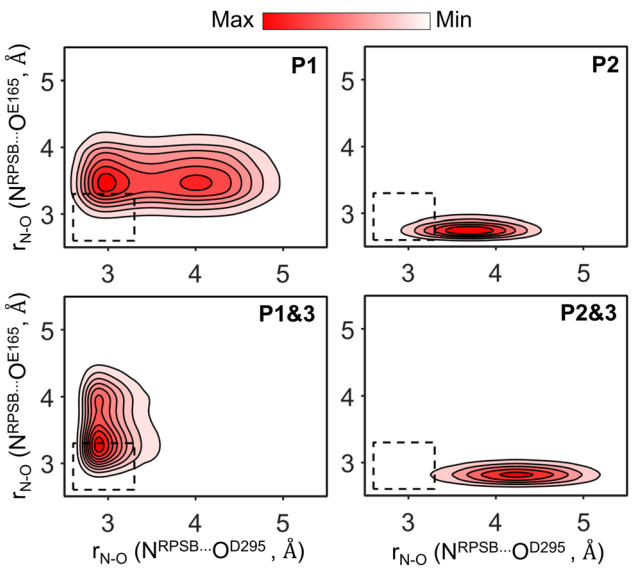

Fig. 3 Kernel density distribution map of the separation between RPSB and the counterions (E165 and D295) in the wild-type. The black (dashed) box denotes the hydrogen-bonding range (between 2.6 and 3.3 Å).

S169A mutant also exhibits the same trend when E132 is protonated (Fig. S4, ESI†). This highlights the importance of the protonation state of this residue, where its protonation resulted in the least structural deviation with respect to the experimental structure. Protonation model P1&3, with E132 and E165 protonated, yields the lowest RMSD values for the protein, the binding pocket, and the retinal chromophore (Fig. S2 and S4, ESI†). We also observed smaller fluctuations of the three counterions in this model (Fig. S1 and S3, ESI†).

Additionally, the interaction between RPSB and the counterions (E165 and D295) was monitored for each protonation model. To this end, the distance between the heavy atoms (Schiff base nitrogen atom and the oxygen atoms of the counterions) was used as an indicator. A kernel density fit was performed to obtain qualitative information about the density around any bond distance between the involved residues. The kernel density distribution map is shown in Fig. 3 and Fig. S5 (ESI†) for the wild-type and the S169A mutant, respectively. Representative structures from the high density region of the kernel distribution for each protonation model are provided in Fig. S6 and S7 (ESI†). RPSB and the counterions were considered to be within the hydrogen-bonding distance if their separation was between 2.6 and 3.3 Å (this region is marked by a dashed box in Fig. 3 and Fig. S5, ESI†). P1&3 (E165 and E132 are protonated) showed the highest density of both counterions interacting with the Schiff base (around 24% and 9% of the simulation time, respectively (Table S1, ESI†)).

Following the classical simulations, a hybrid QM/MM scheme was employed to simulate the absorption spectra of the different protonation models (technical details are provided in the ESI†). The absorption maximum for each model is summarized in Table S2 (ESI†).

To validate the spectral shift between the calculated and the experimental absorption maximum of Chrimson, which depends on the level of theory, Channelrhodopsin-2 (ChR2) was similarly modelled, and its absorption spectrum was calculated as a reference. This choice was made because the protonation states of the titratable residues in this protein have been extensively studied.[27,36–40] The resulting relative shifts between the Chrimson protonation models and ChR2 were then compared to the experimental shift (Fig. 4 and Tables S2, S3, ESI†). The absorption maxima of the S169A mutant models were also generated using the same procedure.

The experimental shift between the absorption maxima of ChR2 and Chrimson was measured to be 0.52 eV, while the S169A mutation induces an additional 0.06 eV red-shift. Model P1&3 was found to best reproduce the experimental shifts for the wild-type (calculated λ_{max} = 601 nm, 2.06 eV), the S169A mutation (calculated λ_{max} = 611 nm, 2.03 eV) and the magnitude of the change between ChR2 and Chrimson. The trend in the energies can be explained based on the electrostatic potential experienced by the retinal chromophore (Fig. 5). The protein environment generates a more negative potential close to the Schiff base in the case of ChR2 as compared to Chrimson (Fig. 5a and b). In the case of the S169A mutant, the Schiff base initially experiencing a negative potential from S169 changes to a positive potential upon mutation to A169, associated with the removal of the polar –OH group (Fig. 5c and d).

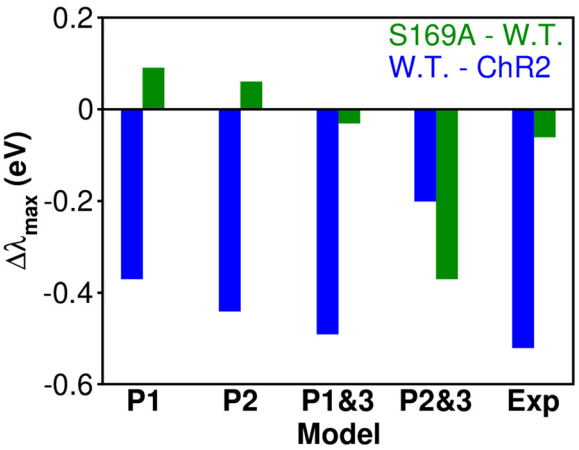

Fig. 4 Spectral shifts of the four different protonation patterns for wild-type (W. T.) and S169A Chrimson. Here, the W. T. model is compared to the simulation of ChR2, while S169A is compared to the simulations of the W. T.

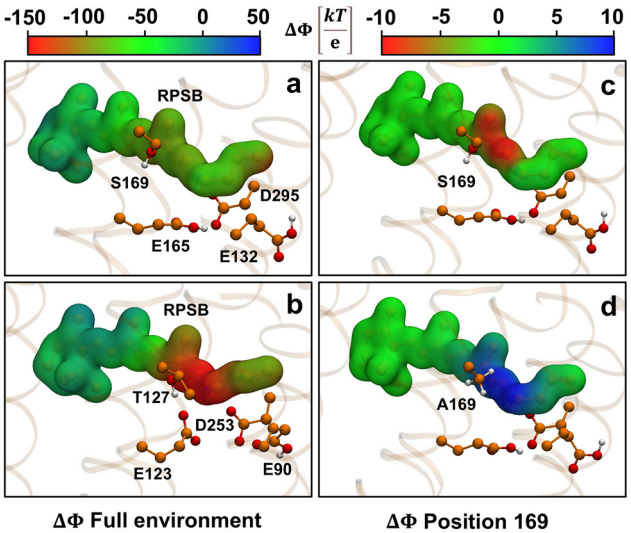

Fig. 5 Electrostatic potential of the protein projected on the retinal PSB. (a) and (b) show the electrostatic potential of the full protein environment on the RPSB in Chrimson (P1&3) and the reference ChR2, respectively. (c) and (d) show the electrostatic potential generated only by the sidechain of S169 and A169 in the Chrimson wild type and the S169A mutant (P1&3), respectively. The protein structures with an excitation energy closest to the computed absorption maximum were used to examine the electrostatic potentials. These maps were generated using APBS in VMD.[41,42]

Models in which E132 was deprotonated, P1 and P2, produced an incorrect trend in the absorption maximum between the wild-type and the S169A mutant with respect to the experiment (Table S2. ESI†). Here, the P1 and P2 wild-type absorption maxima were red-shifted relative to the S169A mutants by 0.09 eV and 0.06 eV, respectively. Protonation of E132 with D295, P2&3 (calculated λ_{max} = 528 nm, 2.35 eV), led to a smaller shift from ChR2 of 0.20 eV and an overestimation of the red-shift from the S169A mutation of 0.37 eV.

Comparison of the spectral shifts in tandem with RMSD analysis relative to the experimental crystal structure strongly

suggests that E132 and E165 are protonated, while D295 should be deprotonated. Interestingly, E132 plays a key role in the correct trends despite not directly interacting with the protonated Schiff base of the chromophore. This combination leads to the lowest overall deviation in the shift and also had the smallest structural deviations relative to the experimental crystal structure. This work emphasizes the importance of critically analyzing the electrostatic environment of the chromophore. These insights can serve as a guide in designing the spectral shift in microbial rhodopsins, as well as in photoactive proteins in general.

I. S. thanks the DFG Collaborative Research Center 1078 (project C6) and Israel Science Foundation, Center of Excellence (grant no. 3131/20), for their support. J. R. C. thanks the Zuckerman STEM Leadership Program for their support. During the revision of this manuscript, two related studies became available. A computational study on Chrimson, and the discovery of a new variant, HulaChrimson.[43,44]

Conflicts of interest

There are no conflicts to declare.

Data availability

The data supporting this article have been included as part of the ESI.†

Notes and references

1 G. Gauvain, H. Akolkar, A. Chaffiol, F. Arcizet, M. A. Khoei, M. Desrosiers, C. Jaillard, R. Caplette, O. Marre, S. Bertin, C.-M. Fovet, J. Demilly, V. Forster, E. Brazhnikova, P. Hantraye, P. Pouget, A. Douar, D. Pruneau, J. Chavas, J.-A. Sahel, D. Dalkara, J. Duebel, R. Benosman and S. Picaud, *Commun. Biol.*, 2021, **4**, 125.
2 V. Emiliani, E. Entcheva, R. Hedrich, P. Hegemann, K. R. Konrad, C. Lüscher, M. Mahn, Z.-H. Pan, R. R. Sims, J. Vierock and O. Yizhar, *Nat. Rev. Methods. Primers*, 2022, **2**, 55.
3 B. Schwarzová, T. Stüdemann, M. Sönmez, J. Rössinger, B. Pan, T. Eschenhagen, J. Stenzig, J. S. Wiegert, T. Christ and F. Weinberger, *Pflügers Arch - Eur. J. Physiol.*, 2023, **475**, 1463–1477.
4 R. A. Bogomolni and J. L. Spudich, *Biophys. J.*, 1987, **52**, 1071–1075.
5 O. Béja, E. N. Spudich, J. L. Spudich, M. Leclerc and E. F. DeLong, *Nature*, 2001, **411**, 786–789.
6 W. Wang, Z. Nossoni, T. Berbasova, C. T. Watson, I. Yapici, K. S. S. Lee, C. Vasileiou, J. H. Geiger and B. Borhan, *Science*, 2012, **338**, 1340–1343.
7 J. Y. Lin, P. M. Knutsen, A. Muller, D. Kleinfeld and R. Y. Tsien, *Nat. Neurosci.*, 2013, **16**, 1499–1508.
8 M. K. Engqvist, R. S. McIsaac, P. Dollinger, N. C. Flytzanis, M. Abrams, S. Schor and F. H. Arnold, *J. Mol. Biol.*, 2015, **427**, 205–220.
9 M. Karasuyama, K. Inoue, R. Nakamura, H. Kandori and I. Takeuchi, *Sci. Rep.*, 2018, **8**, 1–11.
10 M. Broser, A. Spreen, P. E. Konold, E. Schiewer, S. Adam, V. Borin, I. Schapiro, R. Seifert, J. T. M. Kennis, Y. A. Bernal Sierra and P. Hegemann, *Nat. Commun.*, 2020, **11**, 1–10.
11 E. G. Govorunova, O. A. Sineshchekov, H. Li, Y. Wang, L. S. Brown and J. L. Spudich, *Proc. Natl. Acad. Sci. U. S. A.*, 2020, **117**, 22833–22840.
12 A. Rozenberg, I. Kaczmarczyk, D. Matzov, J. Vierock, T. Nagata, M. Sugiura, K. Katayama, Y. Kawasaki, M. Konno, Y. Nagasaka, M. Aoyama, I. Das, E. Pahima, J. Church, S. Adam, V. A. Borin, A. Chazan, S. Augustin, J. Wietek, J. Dine, Y. Peleg, A. Kawanabe, Y. Fujiwara, O. Yizhar, M. Sheves, I. Schapiro, Y. Furutani, H. Kandori, K. Inoue, P. Hegemann, O. Béja and M. Shalev-Benami, *Nat. Struct. Mol. Biol.*, 2022, **29**, 592–603.
13 K. E. Kishi, Y. S. Kim, M. Fukuda, M. Inoue, T. Kusakizako, P. Y. Wang, C. Ramakrishnan, E. F. Byrne, E. Thadhani, J. M. Paggi, T. E. Matsui, K. Yamashita, T. Nagata, M. Konno, S. Quirin, M. Lo, T. Benster, T. Uemura, K. Liu, M. Shibata, N. Nomura, S. Iwata, O. Nureki, R. O. Dror, K. Inoue, K. Deisseroth and H. E. Kato, *Cell*, 2022, **185**, 672–689.e23.
14 M. Broser, *Front. Mol. Biosci.*, 2022, **8**, 806922.
15 N. C. Klapoetke, Y. Murata, S. S. Kim, S. R. Pulver, A. Birdsey-Benson, Y. K. Cho, T. K. Morimoto, A. S. Chuong, E. J. Carpenter, Z. Tian, J. Wang, Y. Xie, Z. Yan, Y. Zhang, B. Y. Chow, B. Surek, M. Melkonian, V. Jayaraman, M. Constantine-Paton, G. K.-S. Wong and E. S. Boyden, *Nat. Methods*, 2014, **11**, 338–346.
16 J. Vierock, S. Rodriguez-Rozada, A. Dieter, F. Pieper, R. Sims, F. Tenedini, A. C. Bergs, I. Bendifallah, F. Zhou, N. Zeitzschel, J. Ahlbeck, S. Augustin, K. Sauter, E. Papagiakoumou, A. Gottschalk, P. Soba, V. Emiliani, A. K. Engel, P. Hegemann and J. S. Wiegert, *Nat. Commun.*, 2021, **12**, 1–20.
17 G. Ciccone, I. Meloni, R. G. Fernandez Lahore, J. Vierock, S. Reineke, H. Kleemann, P. Hegemann, K. Leo and C. Murawski, *Adv. Funct. Mater.*, 2022, **32**, 2110590.
18 S. Kleinlogel, C. Vogl, M. Jeschke, J. Neef and T. Moser, *Physiol. Rev.*, 2020, **100**, 1467–1525.
19 K. Oda, J. Vierock, S. Oishi, S. Rodriguez-Rozada, R. Taniguchi, K. Yamashita, J. S. Wiegert, T. Nishizawa, P. Hegemann and O. Nureki, *Nat. Commun.*, 2018, **9**, 3949.
20 S. Mordechai, N. Koji and H. Barry, *J. Am. Chem. Soc.*, 1979, **101**, 7086–7088.
21 K. Nakanishi, V. Balogh-Nair, M. Arnaboldi, K. Tsujimoto and B. Honig, *J. Am. Chem. Soc.*, 1980, **102**, 7945–7947.
22 B. Honig, U. Dinur, K. Nakanishi, V. Balogh-Nair, M. A. Gawinowicz, M. Arnaboldi and M. G. Motto, *J. Am. Chem. Soc.*, 1979, **101**, 7084–7086.
23 J. Vierock, C. Grimm, N. Nitzan and P. Hegemann, *Sci. Rep.*, 2017, **7**, 9928.
24 D. Urmann, C. Lorenz, S. M. Linker, M. Braun, J. Wachtveitl and C. Bamann, *Photochem. Photobiol.*, 2017, **93**, 782–795.
25 M. Hoffmann, M. Wanko, P. Strodel, P. H. König, T. Frauenheim, K. Schulten, W. Thiel, E. Tajkhorshid and M. Elstner, *J. Am. Chem. Soc.*, 2006, **128**, 10808–10818.
26 K. Fujimoto, S. Hayashi, J.-Y. Hasegawa and H. Nakatsuji, *J. Chem. Theory Comput.*, 2007, **3**, 605–618.
27 Y. Guo, F. E. Beyle, B. M. Bold, H. C. Watanabe, A. Koslowski, W. Thiel, P. Hegemann, M. Marazzi and M. Elstner, *Chem. Sci.*, 2016, **7**, 3879–3891.
28 C. Cheng, M. Kamiya, M. Takemoto, R. Ishitani, O. Nureki, N. Yoshida and S. Hayashi, *Biophys. J.*, 2018, **115**, 1281–1291.
29 M. Tsujimura, T. Noji, K. Saito, K. Kojima, Y. Sudo and H. Ishikita, *Biochim. Biophys. Acta, Bioenerg.*, 2021, **1862**, 148349.
30 R. Liang, J. K. Yu, J. Meisner, F. Liu and T. J. Martinez, *J. Am. Chem. Soc.*, 2021, **143**, 5425–5437.
31 J. R. Church, G. S. Amoyal, V. A. Borin, S. Adam, J. M. H. Olsen and I. Schapiro, *Chem. – Eur. J.*, 2022, **28**, e202200139.
32 L. Pedraza-Gonzalez, L. De Vico, M. D. C. Marin, F. Fanelli and M. Olivucci, *J. Chem. Theory Comput.*, 2019, **15**, 3134–3152.
33 E. Pieri, V. Ledentu, M. Sahlin, F. Dehez, M. Olivucci and N. Ferré, *J. Chem. Theory Comput.*, 2019, **15**, 4535–4546.
34 Y. Guo, F. E. Wolff, I. Schapiro, M. Elstner and M. Marazzi, *Phys. Chem. Chem. Phys.*, 2018, **20**, 27501–27509.
35 D. Di Prima, P. Reinholdt and J. Kongsted, *J. Phys. Chem. B*, 2024, **128**, 2864–2873.
36 G. Nagel, T. Szellas, W. Huhn, S. Kateriya, N. Adeishvili, P. Berthold, D. Ollig, P. Hegemann and E. Bamberg, *Proc. Natl. Acad. Sci. U. S. A.*, 2003, **100**, 13940–13945.
37 K. Sneskov, J. M. H. Olsen, T. Schwabe, C. Hättig, O. Christiansen and J. Kongsted, *Phys. Chem. Chem. Phys.*, 2013, **15**, 7567–7576.
38 S. Adam and A.-N. Bondar, *PLoS One*, 2018, **13**, e0201298.
39 M.-A. Dreier, P. Althoff, M. J. Norahan, S. A. Tennigkeit, S. F. El-Mashtoly, M. Lübben, C. Kötting, T. Rudack and K. Gerwert, *Commun. Biol.*, 2021, **4**, 578.
40 Q. Xin, W. Zhang and S. Yuan, *Int. J. Mol. Sci.*, 2023, **24**, 5667.
41 E. Jurrus, D. Engel, K. Star, K. Monson, J. Brandi, L. E. Felberg, D. H. Brookes, L. Wilson, J. Chen, K. Liles, M. Chun, P. Li, D. W. Gohara, T. Dolinsky, R. Konecny, D. R. Koes, J. E. Nielsen, T. Head-Gordon, W. Geng, R. Krasny, G.-W. Wei, M. J. Holst, J. A. McCammon and N. A. Baker, *Protein Sci.*, 2018, **27**, 112–128.
42 W. Humphrey, A. Dalke and K. Schulten, *J. Mol. Graphics*, 1996, **14**, 33–38.
43 K. Spies, B. M. Bold and M. Elstner, *Phys. Chem. Chem. Phys.*, 2025, **27**, 13360–13370.
44 H. Takahashi, S. Takaramoto, T. Nagata, S. Fainsod, Y. Kato, O. Béjà and K. Inoue, *Biophys. Physicobiol.*, 2025, e220014.

